STEM CELLS AND DEVELOPMENT
Volume 24, Number 10, 2015

DOI: 10.1089/scd.2014.0486

Therapeutic Potential of Gingival Fibroblasts for Cutaneous Radiation Syndrome: Comparison to Bone Marrow-Mesenchymal Stem Cell Grafts

Christine Linard,[1] Frederique Tissedre,[2] Elodie Busson,[2] Valerie Holler,[1] Thomas Leclerc,[2] Carine Strup-Perrot,[1] Ludovic Couty,[3] Bruno L'homme,[1] Marc Benderitter,[1] Antoine Lafont,[3,4] Jean Jacques Lataillade,[2] and Bernard Coulomb[3]

Mesenchymal stem cell (MSC) therapy has recently been investigated as a potential treatment for cutaneous radiation burns. We tested the hypothesis that injection of local gingival fibroblasts (GFs) would promote healing of radiation burn lesions and compared results with those for MSC transplantation. Human clinical-grade GFs or bone marrow-derived MSCs were intradermally injected into mice 21 days after local leg irradiation. Immunostaining and real-time PCR analysis were used to assess the effects of each treatment on extracellular matrix remodeling and inflammation in skin on days 28 and 50 postirradiation. GFs induced the early development of thick, fully regenerated epidermis, skin appendages, and hair follicles, earlier than MSCs did. The acceleration of wound healing by GFs involved rearrangement of the deposited collagen, modification of the Col/MMP/TIMP balance, and modulation of the expression and localization of tenascin-C and of the expression of growth factors (VEGF, EGF, and FGF7). As MSC treatment did, GF injection decreased the irradiation-induced inflammatory response and switched the differentiation of macrophages toward an M2-like phenotype, characterized by $CD163^+$ macrophage infiltration and strong expression of arginase-1. These findings indicate that GFs are an attractive target for regenerative medicine, for easier to collect, can grow in culture, and promote cutaneous wound healing in irradiation burn lesions.

Introduction

Severe local radiation burns from radiological or nuclear incident cause successive but unpredictable inflammatory waves that lead to the horizontal and vertical extension of the necrotic process [1]. The acute response develops over the first few days to weeks after irradiation and is characterized by the early onset of erythema and alopecia, followed soon after by necrosis and ulceration of both cutaneous and subcutaneous tissue [2]. Although several strategies (including surgical procedures) have been used to treat severe radiation-induced skin damage used with some success [2], none has proven entirely satisfactory.

The idea of using stem cell injections to reduce normal tissue injury is not new [3]. More recent studies of wound healing have focused on mesenchymal stem cells (MSCs)—nonhematopoietic, adherent fibroblast-like cells with intrinsic capacity for self-renewal and differentiation—as a possible cell population within the bone marrow that might contribute to cutaneous repair, particularly in radiation burns [4–11].

Wound healing was orchestrated by several temporal processes including hemostasis, inflammation, granulation tissue formation, reepithelialization, and remodeling [12] and was regulated by local production of such growth factors as platelet-derived growth factor (PDGF), epidermal growth factor (EGF), transforming growth factor (TGF-β1), and different vascular endothelial growth factors (VEGF). The resulting effect provided cell proliferation, control of the extracellular matrix (ECM) deposition, and angiogenesis process. In addition to the acceleration of wound closure, the MSCs treatment strongly enhances the scar quality, which was associated to a greater quantity of collagen within the healed tissue increasing the tensile strength [13]. These cells' synthesis of larger amounts of collagen and growth factors, than native dermal fibroblasts, proves their therapeutic efficiency in cutaneous repair [14]. Together, MSC differentiation helps to regenerate damaged tissue, while

[1]Institut de Radioprotection et de Sûreté Nucléaire (IRSN), Fontenay-aux-Roses, France.
[2]Research and Cell Therapy Department, Military Blood Transfusion Center, Percy Military Hospital, Clamart, France.
[3]INSERM UMR 970, PARCC-HEGP, University Paris-Descartes, Paris, France.
[4]Cardiology Department, Hospital Europeen Georges Pompidou, AP-HP, Paris, France.

their paracrine signaling accelerates reepithelialization and fibroproliferation during wound repair [15].

Some points must be considered in planning and assessing MSC-based wound healing therapy. One is that the cells traditionally used are located in bone marrow stroma. The patients' age must also be considered, because stem cell functionality decreases in older patients [16]. Moreover, aspiration of bone marrow from the iliac crest is an invasive procedure. Finally, preparation of MSCs varies between studies [17].

One of the different MSC sources thus far investigated, gingival tissue, has drawn increased interest recently, mainly because it can be obtained from donors noninvasively. Gingival fibroblast (GF) culture, in which $\sim 3\%$ of cells form colonies, expresses membrane markers similar to those of bone marrow-derived MSCs [18,19] and has, like them, immunomodulatory functions and the potential for multilineage differentiation [20,21]. The efficacy of GFs in wound healing was recently shown in a full-thickness skin defect [22]. Still more recently, a suspension of GFs in contact with the arterial wall not only stabilized aneurysms but also caused their regression, with a functional elastin network restored and persisting after 3 months [23]. GFs can be harvested easily and less invasively from gingival mucosa than MSCs obtained from bone marrow. In this study, we investigated the ability of GFs to promote the healing of cutaneous radiation burns and compared it to the reference MSC treatment [5,9].

Materials and Methods

Animals and treatment procedures

NOD-LtSz-scid/scid (NOD/SCID) mice, from breeding pairs originally purchased from Jackson Laboratory, were bred in our pathogen-free unit and maintained in sterile micro-isolator cages with unlimited access to food and drinking water. All experiments and procedures were carried out in accordance with the Guide for the Care and Use of Laboratory Animals published in accordance with the French regulations for animal experiments (Ministry of Agriculture Order No. B92-032-01, 2006) and European Directive 86/609/EEC, and they were approved by the Ethics Committee of the Institute for Radiological Protection and Nuclear Safety.

This study used 60 eight-week-old pathogen-free NOD-SCID mice, divided into eight groups, two not irradiated. Mice were anesthetized with ketamine and xylazine and selectively irradiated at the right hind leg at a dose of 30 Gy (dose rate 1 Gy/min) with a ^{60}Co source. Lead shielding was used to protect the rest of the body from irradiation. Physical dosimetry by thermoluminescent dosimeters indicated that the expected dose was delivered to the right leg and that other parts of the body remained unexposed. Radiation-induced lesions were clearly established 21 days after irradiation, the time chosen as the starting point for cell treatment. Two groups received irradiation only, two groups were irradiated and received hMSC (2.5×10^6) treatment, and two groups were irradiated and received hGF (1.5×10^6). On day 21 after irradiation, under anesthesia, the cell treatments were locally injected into several sites (shin and subcutaneous skeletal muscle) of the irradiated leg. One group with each treatment condition (sham-irradiated, irradiated-untreated, or irradiated and treated with hMSC or GF) was humanely killed on day 28 and the other group on day 50 after irradiation (7 and 29 days after cell treatment).

Isolation and expansion of human MSCs and GFs

Human mesenchymal stem cells. Human bone marrow-derived MSCs were obtained with informed consent from various patients undergoing routine total hip replacement surgery at the Percy Hospital (Clamart, France). The Ethics Committee of the Service de Santé des Armées (Army Health Department, Ministry of Defense) approved this research on human material. As previously reported [9], bone marrow mononuclear cells (BMMNCs) were isolated from the supernatant of spongy bone fragments, plated at a density of 100×10^3 cells/cm^2, and cultured at 37°C in 95% air and 5% CO_2 in alpha-minimum essential medium (α-MEM) (Macopharma) with 10 μg/mL ciprofloxacin (Ciflox 400 mg/200 mL; Bayer Pharma) and 8% human platelet lysate as a source of growth factors. After 3–4 days, nonadherent cells were removed and cultures were again fed with fresh medium. Thereafter, cultures were fed at 3- to 4-day intervals. On days 16–21 after the start of the culture, adherent MSCs reached confluence. They were detached with 1× trypsin-EDTA (Life Technologies, www.lifetechnologies.com) and replated at 4,000 cells/cm^2. Expanded MSCs were validated for their standard phenotypic markers by flow cytometry ($CD45^-/CD105^+/CD73^+/CD90^+$), their colony-forming unit-fibroblast potential (CFU-F assay), and their multilineage differentiation potential (osteogenic, adipogenic, and chondrogenic).

Human gingival fibroblasts. Gingival tissue samples were obtained from healthy patients undergoing extraction of the third molar or orthodontic procedures. The study was approved by the local ethics committee (Comité de Protection des Personnes (CPP) ''Ile de France II'' (May 11, 2012), IRB registration: 00001072) and all subjects gave written informed consent. As previously reported [19,21], primary explant cultures were established in Dulbecco's modified Eagle's medium (DMEM) containing 5% human platelet lysate, penicillin (100 μg/mL), streptomycin (100 μg/mL), and amphotericin B (2 ng/mL) over 2-week periods. Monolayer cultures were maintained in 5% CO_2 and the cell culture medium was changed every 72 h. After 2 weeks, the GFs were trypsinized and single-cell suspensions were seeded at very low concentrations (≤ 100 cells/cm^2; medium, DMEM 10% of FBS with 50 mg/mL of ascorbic acid) after verification of the absence of cell aggregates to avoid false positives. After 14 days of culture, the CFU-F were counted; only aggregates of >50 cells were considered colonies. The CFU-F were then transferred, pooled in a single 25-cm^2 flask, and cultivated in DMEM 10% supplemented with 50 mg/mL of ascorbic acid. Expanded GFs were tested to check that they expressed the same markers as the BM-MSCs ($CD29^+/CD44^+/CD105^+/CD73^+/CD90^+/CD45^-$) and for their multilineage differentiation potential (osteogenic, adipogenic, and chondrogenic).

Histology and immunohistochemistry

Freshly isolated tissue was fixed in 4% paraformaldehyde and embedded in paraffin. Sections 5 μm in thickness were dewaxed and hydrated; endogenous peroxidase was blocked

with 3% hydrogen peroxide for 10 min; and nonspecific binding was blocked with a protein blocker (DakoCytomation, www.dakocytomation.com). Masson trichrome staining by the standard method was used to assess collagen deposition. After antigen retrieval, sections were incubated in primary antibodies against α-SMA, CTGF, tenascin-C, F4/80 (AbCam), and CD163 (Antibodies-Online.com, www.antibodies-online.com). The EnVision$^+$ System-horseradish peroxidase (HRP) (DakoCytomation) was used as the secondary reagent for all immunostaining sections. The color reaction was developed with the NovaRED™ kit (Vector Laboratories, www.vectorlabs.com) and counterstained with Mayer's hemalun.

Detection of hBMSC and hGF in irradiated tissue

A real-time PCR-based assay was used to detect the presence of human cells in the tissue of mice receiving hMSC or hGF infusions. Genomic DNA was extracted from skin samples by the DNEasy method (Qiagen, www.qiagen.com); a 1-μg aliquot of total DNA was used in each PCR reaction, all run on an ABI Prism 7900 sequence detection system. System genomic DNA from the human cells was amplified with primers directed against GAPDH (Hs00894322_cn; Life Technologies) and HPRT (Hs05632001_cn; Life Technologies). A genomic DNA sequence located in the noncoding region of the beta-2 microglobulin locus (Mm00047666_cn; Life technologies) was used as an internal control. All PCR experiments were performed with appropriate controls, including absence of HuGAPDH and HuHPRT in mice not treated with human cells.

Real-time PCR analysis

Total RNA was extracted from cultured hGF, hMSC, and the anus, rectum, and colon with the RNeasy Mini kit (Qiagen), and cDNA prepared with the SuperScript RT Reagent Kit (Life Technologies). Real-time PCR was performed on an ABI Prism 7900 sequence detection system. SYBR chemistry (Life Technologies) was used to amplify PCR, with primers specific for Col3a1 (F:5′-AACCTGG TTTCTTCTCACCCTTC-3′; R:5′-ACTCATAGGACTGAC CAAGGTGG-3′); TGF-β1 (F:5′-CACAGTACAGCAAGG TCCTTGC-3′; R:5′-AGTAGACGATGGGCAGTGGCT-3′); VEGF (F:5′-CATCTTCAAGCCGTCCTGTGT-3′; R:5′-CT CCAGGGCTTCATCGTTACA-3′); CD68 (F:5′-TTGGGAA CTACACACGTGGGC-3′; R:5′-CGGATTTGAATTTGGG CTTG-3′); MCP1 (F:5′-CTTCTGGGCCTGCTGTTCA-3′; R:5′-CCACTCATTGGGATCAGCCTA-3′); and iNOS (F:5′-CATTGGAAGTGAAGCGTTTCG-3′; R:5′-CAGCTGGGCT GTACAAACCTT-3′). All other TaqMan primers and probes came from Life Technologies. Data were analyzed by the $2^{-\Delta\Delta Ct}$ method, with normalization to the Ct of the housekeeping gene GAPDH (glyceraldehyde 3-phosphate dehydrogenase).

Enzyme-linked immunosorbent assay

Tissues were homogenized in a cold RIPA buffer (Sigma) containing a standard protease-inhibitor cocktail. The samples were then centrifuged at 10,000 *g* for 10 min, and the supernatants stored at −20°C for later measurement. Human and mouse TIMP1 concentrations were determined by specific enzyme-linked immunosorbent assay (ELISA) according to the manufacturer's instructions (R&D Systems). Any cross-reaction between human and mouse was detected.

Statistics

Data are expressed as means ± SEM. One-way analysis of variance was used followed by a Bonferroni post-test to determine the significance of differences. *P* values less than 0.05 were considered statistically significant.

Results

Gene expression of transplanted MSCs and GFs

RT-PCR analysis was performed to investigate the relative mRNA expression levels of selected growth factors, cytokines and chemokines associated with inflammation, neovascularization and reepithelialization, and/or remodeling in injected BM-MSCs and GF. As shown in Fig. 1 and compared to mRNA expression levels of injected MSC, GF repressed inflammatory cytokine/chemokines (Il-1β, CCl5, and CXCL2) and overexpressed anti-infammatory cytokine IL1-Ra (13-fold), angiogenesis factors (angiotensinogen, 11.8-fold; endothelin 1, 7-fold; thrombomodulin, 5.5-fold; VWF, 3.5-fold), and remodeling factors (fibroblast activation protein a, 3-fold, S100A4, 4.3-fold; TGF-β2, 9.5-fold; membrane metallo endopeptidase, 10-fold and Noggin, 26.5-fold).

Persistence of transplanted MSCs and GFs in irradiated skin

Real-time PCR was used to detect genomic DNA (directed against the GAPDH and HPRT of human MSCs or GFs) from irradiated mouse skin samples collected 7 and 29 days after cell injection (days 28 and 50 after irradiation). At 7 days, human-derived cells were detectable by PCR in 50% of mouse skins after MSC treatment and in 60% after GF treatment; the corresponding results at 29 days were 40% and 60%, respectively. After determining that human TIMP1 did not cross-react with that of mice (no hTIMP1 protein was detected in nonirradiated or irradiated-untreated mice), we immunoassayed hTIMP1 in the skins of treated mice and found that its concentration decreased over time after MSC treatment, but remained high at 29 days after GF treatment (Table 1). Together, these results showed that GFs persist longer in tissue than MSCs.

Effects of MSCs and GFs on collagen content in irradiated skin

The ability of MSCs and GFs to regenerate skin repair was evaluated in cutaneous radiation lesions after subcutaneous cell transplantation. Macroscopic images and histologic assessment of tissue sections stained with Masson's trichrome dyes revealed cutaneous ulceration and failed epithelialization on day 28 after irradiation in the irradiated-untreated group (Fig. 2A, B). Although the wound site was covered on day 50, hyperplasia of the epidermis was observed, marked by extensive hyperkeratosis, atrophy of the dermal appendages, a drastic reduction in the number of hair follicles and sebaceous glands, and atrophy of those that remained (Fig. 2B). On day 28 (7 days after transplantation), the GF-treated mice had notably less epidermal hyperplasia,

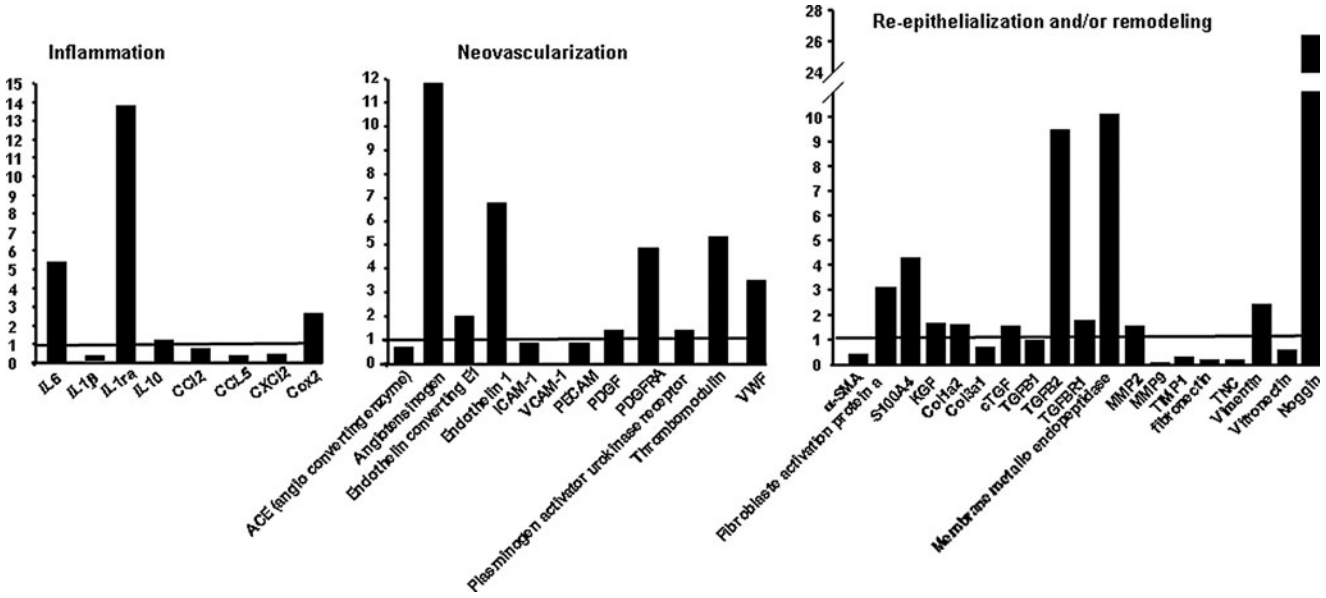

FIG. 1. mRNA expression levels of GF compared to BM-MSCs before transplantation. Real-time PCR assays were performed to measure mRNA levels of inflammatory, neovascularization, and remodeling factors in GF compared to BM-MSCs. The fold changes were generated by comparing cultured hGF (histogramme) with hMSCs (basal line to 1). GAPDH was quantified as an internal control. MSC, mesenchymal stem cell; GF, gingival fibroblast; Irr, irradiation.

restored dermal appendages, and more hair follicles. The MSC treatment induced the same effect, but at a later point in time, on day 50 (29 days after the graft), although the anagen phase occurs earlier than with GF treatment. Analysis of the overall collagen content showed a high density of dermal collagen fibers with unidirectional alignment in the control irradiated skin on days 28 and 50 (Fig. 2C). The restoration of normal fiber density and their multidirectional alignment (remodeling), resembling nonirradiated skin, was visible on day 28 in the GF-treated skin but not until day 50 in the MSC-treated skin. Histomorphometric analysis showed that the earliest signs of tissue regeneration appeared earlier in GFs than MSCs.

To evaluate the molecular effects of MSCs and GFs on matrix production, we used real-time PCR to measure expression of collagen 1 and 3, which constitute the bulk of the scar tissue ECM. Irradiation significantly increased the collagen 3 expression observed on days 28 and 50 (two and three-fold respectively, $P < 0.01$), compared with nonirradiated skin (Fig. 2D). This overexpression continued on day 28 after both MSC ($\sim$4.8-fold) and GF ($\sim$3-fold) treatment but returned to normal by day 50. Collagen 1 expression, on the contrary, was unaffected by irradiation but significantly increased after MSC and GF treatment on day 28 (2.6 and 3-fold respectively, $P < 0.01$), compared with nonirradiated and irradiated skin. The resulting ratio of collagen I/III is an indicator of tissue quality, which was poor (0.2 on day 28 and 0.4 on day 50) in irradiated-untreated compared to nonirradiated skin. For GF-treated skin, this ratio had returned to normal levels by day 28, and for MSC-treated skin, by day 50.

Table 1. Persistence of Transplanted Mesenchymal Stem Cells or Gingival Fibroblast in Irradiated Skin

	Control	*Irr*	*Irr+MSC*	*Irr+GF*
% of mouse with human-derived cells detected				
D28	ND	ND	50%	60%
D50	ND	ND	40%	60%
Human TIMP in mouse tissue (ng/mL)				
D28	ND	ND	78.4 ± 18.3	153.5 ± 46.0
D50	ND	ND	29.5 ± 13.0	83.6 ± 26.6

GF, gingival fibroblast; Irr, irradiation; MSC, mesenchymal stem cell; ND, not detected.

MSCs and GFs modified ECM-related gene expression

MMPs degrade collagens, and TIMPs inhibit MMP activity. For this reason, we performed real-time PCR to examine the expression of several MMPs and TIMP1. MMP2 expression was transiently increased on day 28 in irradiated-untreated mice (Fig. 3A), but normalized by that time in GF-treated mice. Irradiated-untreated mice strongly overexpressed both MMP3 and MMP13 on both day 28 and 50 postirradiation; their levels were also elevated at both time points in MSC- and GF-treated mice. Similarly, TIMP1 expression was strongly overexpressed on day 28 in the skin of irradiated mice, although transiently (Fig. 3B). This enhanced TIMP1 expression persisted in MSC- and GF-treated mice, on both day 28 and 50. The ELISA assay confirmed this finding at the protein level.

Because collagen synthesis/degradation depends on the dynamic interactions of these proteins, their relation was assessed by the collagen-to-MMP-to-TIMP ratio, a method of defining net collagen deposition based on real-time PCR results [24]: the collagen mRNA value is divided by the fold change value for the relevant MMPs and TIMPs (Fig. 3C). The collagen/MMPP:TIMP ratio is 1 for nonirradiated skin, which is assumed to have no net collagen deposition or

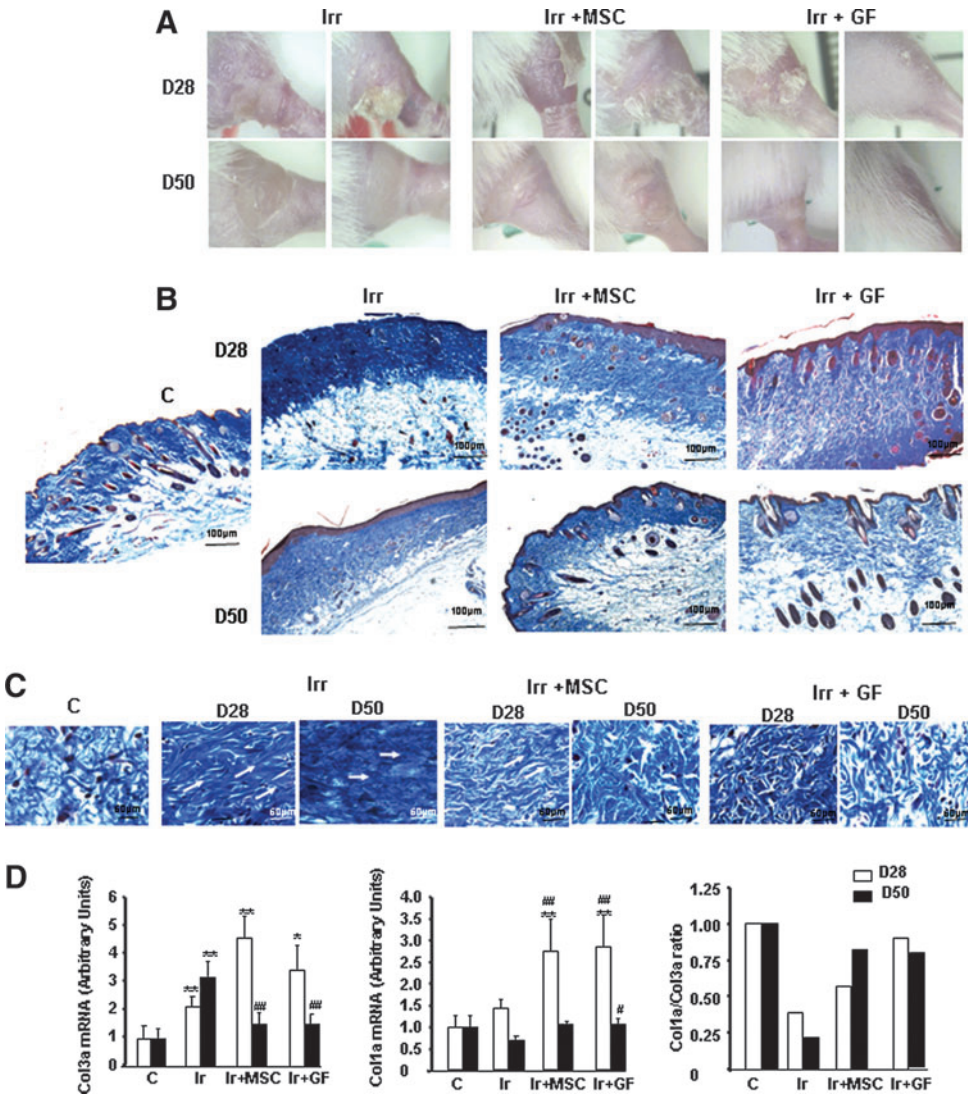

FIG. 2. MSCs and GFs modified radiation-induced collagen deposition. **(A)** Representative macroscopic pictures, **(B)** Masson trichrome staining in irradiated groups, MSC-treated groups, and GF-treated groups on days 28 and 50 after irradiation. ×20 magnification. **(C)** Staining revealed a high density of dermal collagen fibers with unidirectional alignment parallel to the *white arrows* after irradiation and the restoration of multidirectional alignment after MSC or GF treatment. **(D)** Real-time PCR of Col3a, Col1a, and Col1a/Col3a ratio. Data are expressed relative to control mice and normalized to GAPDH. Results are expressed as mean ± SEM. *P* values were calculated by analysis of variance (ANOVA) with Bonferroni correction, $^{*}P < 0.05$; $^{**}P < 0.01$ compared with nonirradiated controls; $^{\#}P < 0.05$; $^{\#\#}P < 0.01$ compared with irradiated-untreated controls.

degradation. For collagen 1 and 3, the net collagen/MMPP:TIMP ratio was elevated after MSC and GF treatment, and significantly higher in GF-treated compared to irradiated-untreated mice on day 28.

MSCs and GFs modulated the expression of ECM components

Tenascin-C is regarded as a marker for immature ECM in the earlier phase of tissue repair and plays an important role in myofibroblast recruitment [25]: the dramatic change in its expression demonstrates its key role in the wound healing process. Real-time PCR showed significant overexpression of tenascin-C in irradiated-untreated skin on both days 28 and 50 ($P < 0.001$). MSC treatment did not modify the irradiation-induced enhancement of tenascin-C expression, but its level on day 28 was significantly lower in GF-treated mice (Fig. 4A). In nonirradiated skin, immunostaining detected tenascin-C mainly in the nascent hair follicle and bulge stem cells (Fig. 4B). On day 28 in irradiated-untreated mouse skin, tenascin-C staining was marked at the dermal–epidermal junction and around the residual hair follicles. At this early point in MSC-treated skin, the tenascin-C staining showed a continuous distribution in the basement membrane of the dermal–epidermal junction and in the dermis, mostly close to hair follicles. GF-treated skin, on the other hand, showed discontinuous tenascin-C staining in the dermal–epidermal junction and in part around the hair follicles. On day 50, the irradiated-untreated skin showed intense tenascin-C staining at the dermal–epidermal junction and in the adjacent dermis, where collagen fibers were organized parallel to the wound surface. At this point, the detection of tenascin-C staining in the MSC-treated skin was discontinuous at the dermal–epidermal junction and in the nascent hair follicles and bulge stem cells, while that in GF-treated skin was similar to that in the skin of nonirradiated mice.

In view of previous reports that tenascin-C promotes recruitment of myofibroblasts [26], we assessed the localization of α-smooth muscle actin (SMA) by immunostaining. In the dermis of nonirradiated skin, α-SMA was expressed close to the perifollicular dermal sheath area and vascular wall (Fig. 4C). Irradiated mouse skin (assessed on days 28 and 50 after irradiation) showed stronger α-SMA staining in the dermis. In mice treated with MSCs, α-SMA-positive cells were located near the vascular wall on day 28. In GF-treated mice, as in the nonirradiated mice, α-SMA was

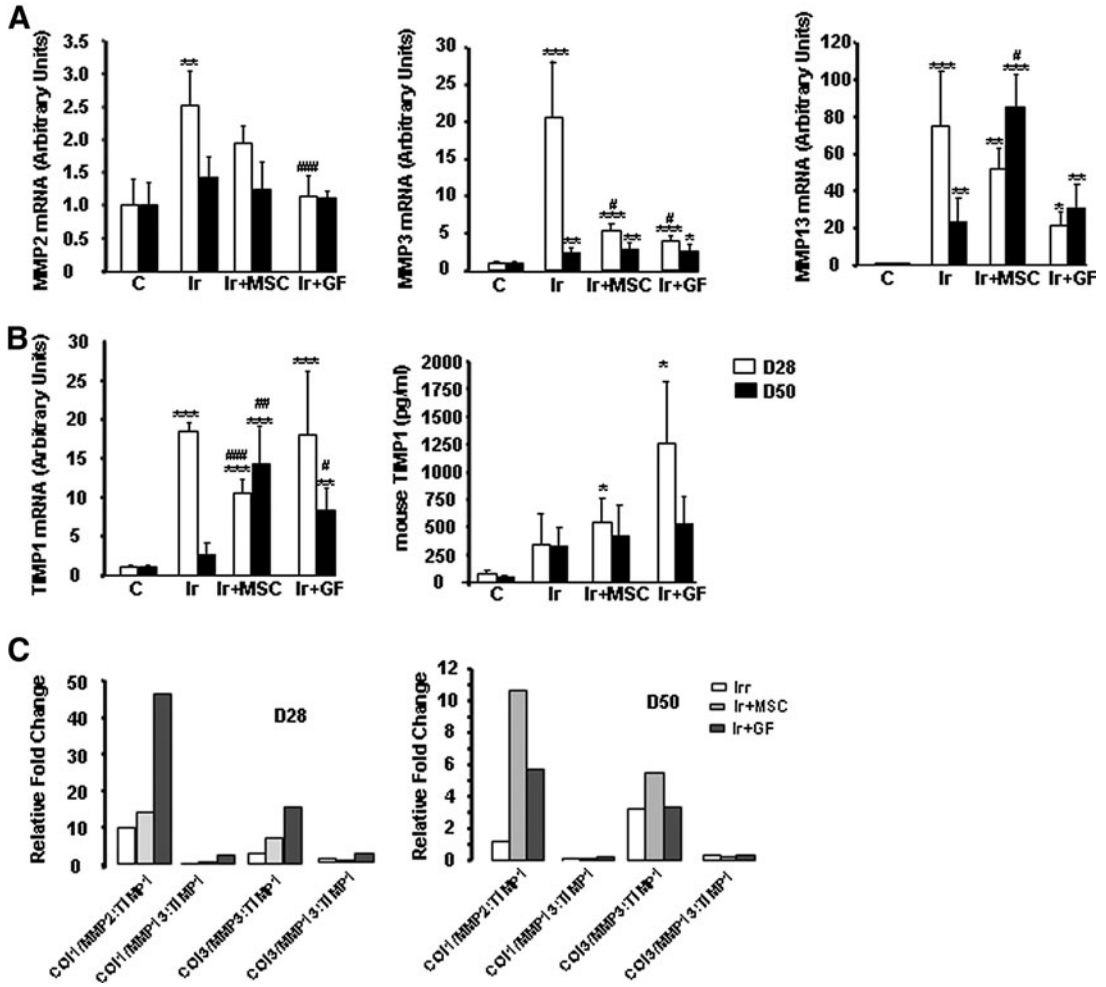

FIG. 3. MSC or GF treatment influences ECM remodeling. **(A)** Real-time expression of MMP-2, MMP-3, and MMP-13. **(B)** TIMP-1 mRNA and protein expression. Levels of mRNA are expressed relative to control mice and normalized to GAPDH. Protein was measured in skin by ELISA test. **(C)** Collagen-to-MMP-to-TIMP ratio: relative expression of MMP was calculated by determining the fold change of MMP mRNA levels relative to its relevant inhibitor TIMP in irradiated-untreated and irradiated MSC- and GF-treated groups on days 28 and 50 after irradiation, compared with control groups. Results are expressed as mean ± SEM. *P* values were calculated by ANOVA with Bonferroni correction, $^{*}P<0.05$; $^{**}P<0.01$; $^{***}P<0.001$ compared with nonirradiated controls; $^{\#}P<0.05$; $^{\#\#}P<0.01$; $^{\#\#\#}P<0.001$ compared with irradiated-untreated controls. ECM, extracellular matrix.

expressed near the perifollicular dermal sheath by day 28, and in MSC-treated mice by day 50.

Expression of wound healing-related factors in wounded tissue

TGF-β1 and CTGF, working synergistically, and PAI-1 play active roles in fibroblast-to-myofibroblast activation and matrix deposition, in addition to negative roles in wound reepithelialization. For that reason, we used real-time PCR to analyze their expression in irradiated-untreated and irradiated-treated skin (Fig. 5A). On day 28, TGF-β1 expression did not differ in irradiated-untreated, irradiated MSC- and GF-treated, or sham-irradiated mice. Also at this point, CTGF expression significantly decreased in the skin of all three irradiated groups. On day 50, expression of both TGF-β1 and CTGF was significantly higher in the skin of irradiated-untreated mice than in nonirradiated mice. Expression of TGF-β1 had normalized at that point in GF-treated skin and that of CTGF in both MSC- and GF-treated skin. Similarly, both treatments reduced the increased PAI-1 expression observed in irradiated-untreated skin—a 3-fold increase on day 28 and 23-fold on day 50, compared with nonirradiated skin. Immunostaining confirmed that both MSC and GF treatment substantially reduced the intensity of CTGF staining observed in the dermis on day 50 in irradiated-untreated skin near the perifollicular dermal sheath area (Fig. 5B).

Other growth factors, such as VEGF, FGF7, and EGF, have been implicated in wound repair [27]. Consistent with these reports, VEGF expression was significantly enhanced on day 28 by GF treatment and on day 50 by MSC treatment, compared with irradiated-untreated skin (Fig. 6A). Moreover, endothelial nitric oxide synthase expression also tended to return to normal levels by day 28 in GF-treated skin. EGF and FGF7 expression was significantly modified

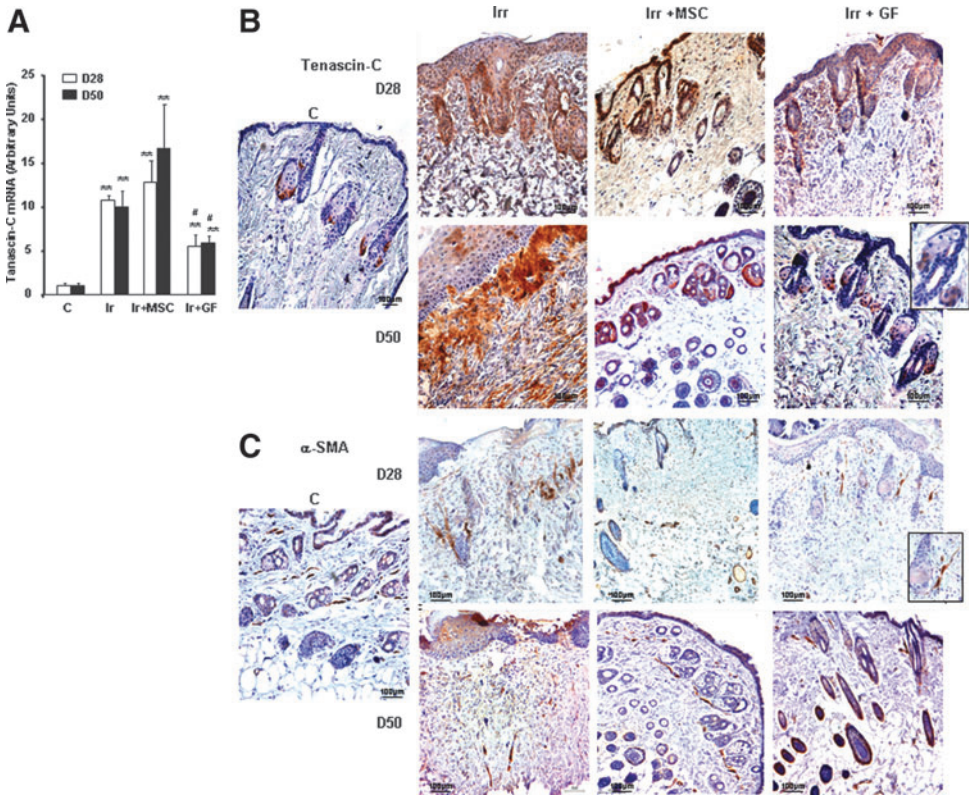

FIG. 4. Expression of ECM components. **(A)** Real-time PCR of tenascin-C in nonirradiated control skin, irradiated-untreated skin, and MSC- or GF-treated skin on days 28 and 50 after irradiation. Data are reported relative to control mice and normalized to GAPDH. **(B)** Representative immunohistochemical staining with the primary anti-tenascin-C antibody and **(C)** the primary α-SMA antibody. *Inserts* were amplified local areas from the same images. Original magnification ×20. Results are expressed as mean ± SEM. *P* values were calculated by ANOVA with Bonferroni correction, $^{**}P < 0.001$; compared with nonirradiated controls; $^{\#}P < 0.01$ compared with irradiated-untreated controls.

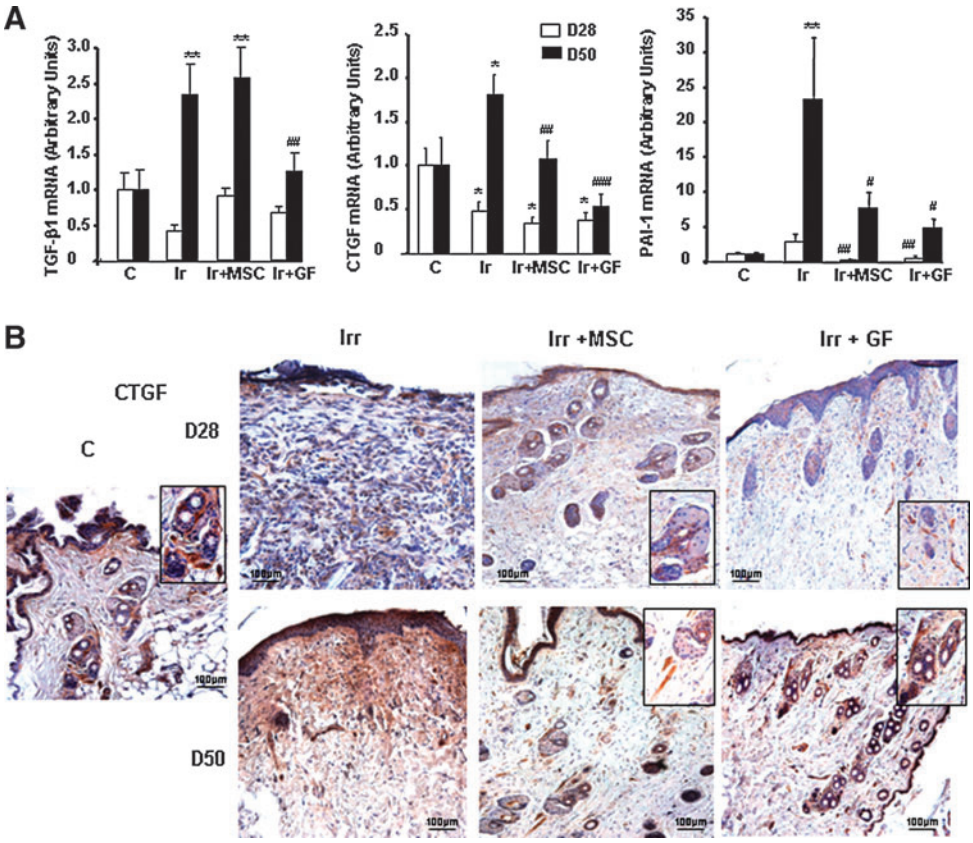

FIG. 5. Expression of wound healing-related factors. **(A)** Real-time PCR of TGF-β, CTGF, and PAI-1 in nonirradiated control skin, in irradiated-untreated skin, and in MSC- or GF-treated skin on days 28 and 50 after irradiation. Data are reported relative to control mice and normalized to GAPDH. **(B)** Representative immunohistochemical staining with the primary CTGF antibody. Inserts were amplified local areas from the same images. Original magnification ×20. Results are expressed as mean ± SEM. *P* values were calculated by ANOVA with Bonferroni correction, $^{*}P < 0.05$; $^{**}P < 0.01$ compared with nonirradiated controls; $^{\#}P < 0.05$; $^{\#\#}P < 0.01$; $^{\#\#\#}P < 0.001$ compared with irradiated-untreated controls.

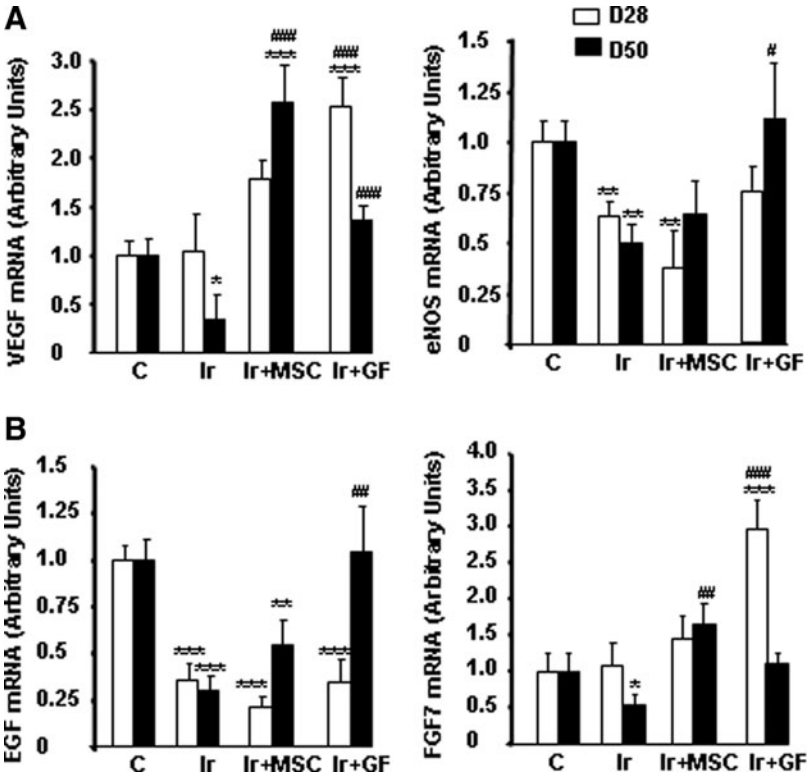

FIG. 6. Expression of growth factors implicated in wound repair. Real-time PCR of VEGF and eNOS **(A)** and EGF and FGF7 **(B)** in nonirradiated control skin, in irradiated-untreated skin, and in MSC- or GF-treated skin on days 28 and 50 after irradiation. Data are reported relative to control mice and normalized to GAPDH. Results are expressed as mean ± SEM. *P* values were calculated by ANOVA with Bonferroni correction, $^{*}P<0.05$; $^{**}P<0.01$; $^{***}P<0.001$ compared with nonirradiated controls; $^{\#}P<0.05$; $^{\#\#}P<0.01$; $^{\#\#\#}P<0.001$ compared with irradiated-untreated controls. eNOS, endothelial nitric oxide synthase.

in irradiated-untreated skin (Fig. 6B). Only GF treatment normalized EGF expression ($P<0.01$ compared to irradiated skin). Although FGF7 was upregulated on day 28 in mice with GF transplants, the mRNA level returned to normal only on day 50 after irradiation in MSC-treated skin.

Macrophage recruitment induced by MSC and GF treatment promotes alternative activation

Previous studies have established that macrophages enter sites of tissue injury, where they facilitate angiogenesis and promote wound repair [28]. We used real-time PCR to evaluate the local anti-inflammatory effect of MSC and GF treatment (Fig. 7A). The overexpression of IL-6 and IL-1β induced by irradiation was significantly downregulated after one week of MSC or GF treatment (D28). ELISA assays also confirmed the decrease in IL-1β at the protein level in mice treated with MSCs and GFs on both days 28 and 50 postirradiation.

Compared with nonirradiated skin, irradiated-untreated skin in addition to MSC- and GF-treated skin had higher numbers of cells that stained for the macrophage marker F4/80 (Fig. 7B). Real-time PCR confirmed the overexpression of CD68 and the monocyte chemoattractant protein-1 (MCP1) in all three types of irradiated skin on day 28 and 50 (Fig. 7C). To determine whether the macrophages present after MSC or GF transplantation phenotypically differed from those present after irradiation, we used real-time PCR to assess the expression of inducible nitric oxide synthase (iNOS) (marker of the M1 proinflammatory macrophages) and Arginase-1 (Arg-1, expressed by the M2 alternatively activated macrophages). As Fig. 7D shows, inducible nitric oxide synthase expression increased by a factor of 90 ($P<0.001$) on day 28 and of 8 ($P<0.05$) on day 50. Arg-1 expression did not differ in irradiated compared to nonirradiated skin. MSC or GF treatment substantially reduced iNOS expression at both time points, while Arg-1 expression on days 28 and 50 increased compared with irradiated-untreated skin. Analysis of the ratio of iNOS/Arg-1 mRNA levels, an indicator of the M1/M2 activity balance [29], showed that irradiation skewed this ratio toward iNOS expression. After either MSC or GF treatment, this ratio markedly decreased and skewed back toward Arg-1 expression, compared with irradiated-untreated skin. Immunostaining of $CD163^{+}$ cells showed that the number of M2 macrophages increased after MSC or GF administration, compared with nonirradiated and irradiated-untreated skin (Fig. 7E).

Discussion

The clinical benefits of local MSC grafts in promoting healing of radiation burn lesions have been demonstrated in several different preclinical models [7,8] and in humans [5,9]. The healing of skin wounds involves complex interactions between different cell types, including fibroblasts and epithelial, endothelial, and inflammatory cells, ECM molecules, growth factors, and cytokines [4]. We investigated the performance of GF tissue grafts in wound healing and compared it to the reference MSC therapy, using a local irradiation model, human bone marrow-derived MSCs, and GFs, expanded according to a clinical-grade protocol.

GFs express mesenchymal cell surface markers and are capable of multiple mesodermal differentiations. Interestingly, GFs injected near the lesion remained detectable for a longer time after grafting than did bone marrow-derived MSCs. This observation confirms a previous report in an aneurysm model where GFs remained detectable 3 months after cell therapy, although more than 90% of the injected MSCs disappeared in the first few days [23].

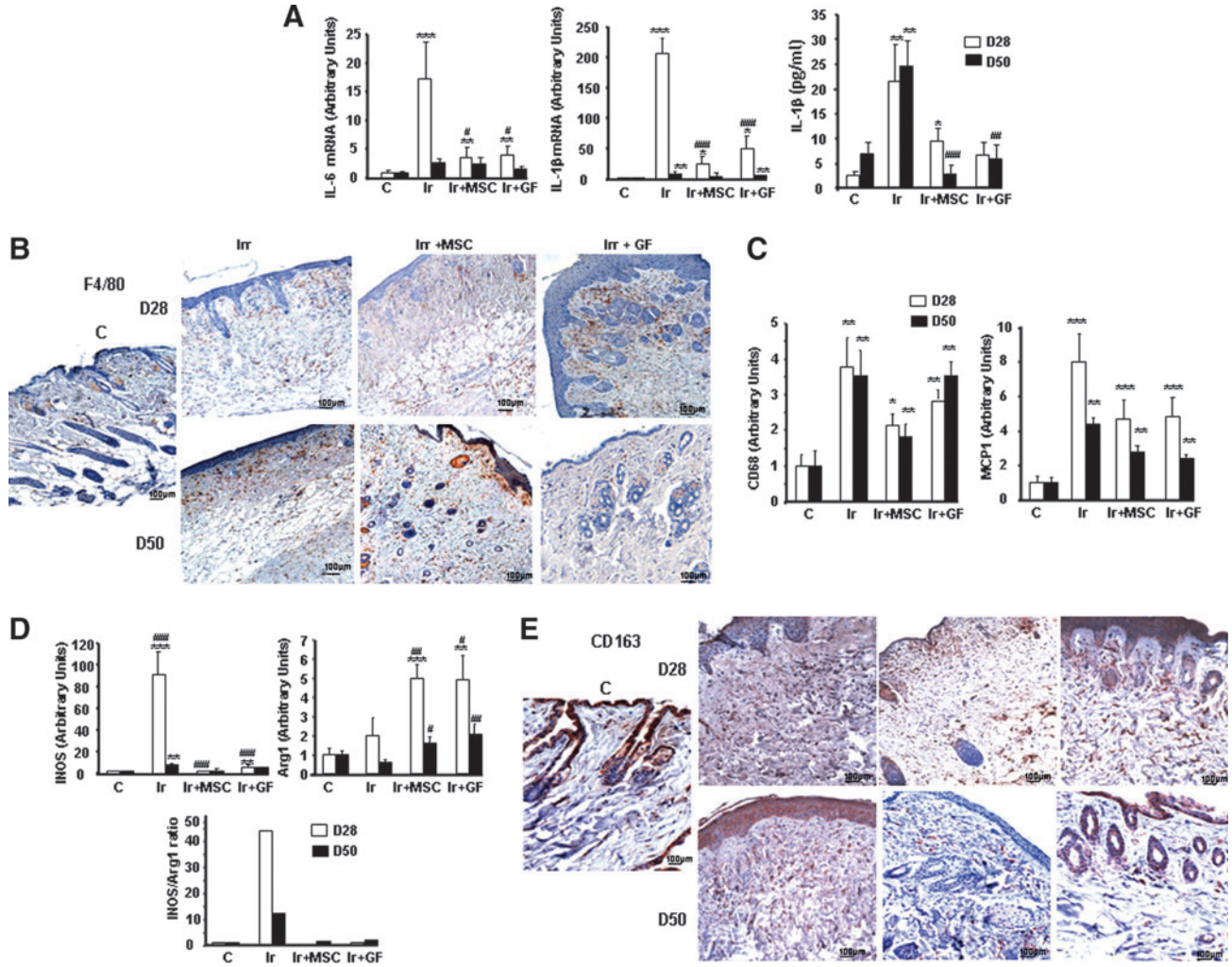

FIG. 7. Modification of inflammatory profile by MSC or GF treatment. **(A)** Real-time-PCR analysis of IL-6 and IL-1β. Protein level of IL-1β was analyzed in skin by ELISA test. **(B)** Representative immunostaining for F4/80-positive macrophages. **(C)** Real-time PCR analysis of CD68, MCP1, genes related to macrophage infiltration. **(D)** Real-time PCR analysis of genes related to M1 macrophage iNOS and M2 macrophage activity Arg-1 and iNOS/Arg-1 mRNA level ratio as an index of M1/M2 activity balance. **(E)** Representative immunostaining of CD163. Original magnification ×20. Results are expressed as mean ± SEM. *P* values were calculated by ANOVA with Bonferroni correction, $^{*}P<0.05$; $^{**}P<0.01$; $^{***}P<0.001$ compared with nonirradiated controls; $^{\#}P<0.05$; $^{\#\#}P<0.01$; $^{\#\#\#}P<0.001$ compared with irradiated untreated controls. iNOS, inducible nitric oxide synthase.

A specific series of events occurs during the closure and repair of wounds caused by radiation. These events include an inflammatory step due to the monocytes/macrophages infiltration, secretion of cytokines/chemokines, cell migration, differentiation of fibroblasts to myofibroblasts, and synthesis/accumulation of collagen and other ECM proteins in the matrix. The magnitude of ECM protein accumulation is tightly controlled by the balance between the synthesis of ECM and its degradation.

The histological changes we observed in our murine model were typical of irradiated skin (epidermal atrophy, hyperkeratosis, atrophy of dermal appendages, hair follicle sterilization, and unidirectional alignment of collagen fibers) [30]. Histological evaluation of the wound in GF-treated skin after only one week of treatment revealed early development of thick, fully regenerated epidermis, skin appendages, and the presence of hair follicles. In MSC-treated skin, in contrast, appendages had not yet developed at this point, and hair follicles were present in the earliest anagen state; epidermal thickness and appendages were nonetheless similar to that of nonirradiated skin only 3 weeks after treatment. The arrangement of the deposited collagen in different directions, in a network similar to that of control skin, took place later in MSC-treated skin than in GF-treated skin.

Wound maturity is related to the initial deposition of thin collagen 3, with type 1 collagen prevalent only later [31]. Type 3 collagen are abundant in young granulation and scar tissue while the type 1 collagen is few present in this early phase of healing. The ratio of type 1 to type 3 collagen is thus low. Although collagen 1 overexpression was observed as early as day 28 postirradiation in both MSC and GF treatment normalization of the ratio was observed later in MSC treatment; this finding indicates delayed healing compared to GF treatment. As previously reported, though

type 1 and type 3 collagen fibers coexist within individual fibrils, their relative ratios play an important role in the regulation of fibrillogenesis and in the determination of the final fibular diameter and bundle architecture [32]. The mature type 1 collagen is responsible for mechanical stability, whereas the type 3 collagen that forms thin fibers can be regarded as immature collagen of the early wound healing process. MMPs and TIMPs perform this stage of wound repair-remodeling. In our study, the maximum collagen-to-MMP-to-TIMP ratios—on day 28 in GF-treated skin and on day 50 in MSC-treated skin—confirm the peak time of collagen production.

Tenascin-C, which is transiently upregulated during the proliferative phase of healing and is predominantly produced by fibroblasts, virtually disappears in mature tissue [25]. In our study, irradiation induced strong tenascin-C expression localized at the dermal–epidermal junction. In the mice treated by MSCs and GFs, real-time PCR analysis showed that tenascin-C expression remained high compared to nonirradiated mice, but immunostaining revealed discontinuous localization in the dermal–epidermal junction, mostly close to hair follicles. Some reports indicate that tenascin-C is present throughout the matrix of granulation tissue, filling full-thickness wounds, but it is not detectable in the scar after the completion of wound contraction [33]. Tenascin-C may also interact with the contractile properties of myofibroblasts to influence wound contraction. In our study, α-SMA immunostaining indicated an increase of myofibroblasts in the dermis of irradiated-untreated skin. In MSC- or GF-treated skin, on the other hand, myofibroblast immunostaining decreased and was restricted to hair follicles. Our findings are thus in line with the report of tenascin-C involvement in myofibroblast recruitment [26]; the presence of tenascin-C on day 50 postirradiation in our study signals immature tissue granulation and on-going migration. MSC and GF treatment thus appear to have accelerated the wound healing process, with tenascin-C rapidly disappearing after wound contraction was complete [33]. The α-SMA$^+$ myofibroblasts are present in the early stage of the wound, and they rapidly disappear when wound healing progresses [34]. An interesting recent study reports that whisker follicle stem cell niches contain tenascin-C and suggests that this glycoprotein might play a role in directing the migration and proliferation of these stem cells [35]. In our study, the presence of tenascin-C close to hair follicles may predict hair stem cell niche restoration by MSC and GF treatment.

It is generally accepted that the efficacy of MSC transplantation is associated with the immunomodulatory activity of these cells [36]. Similarly, GF cell therapy has recently been associated with a reduction in proinflammatory cytokines [23]. We have shown here a significant down-regulation of IL-1β and IL-6 in irradiated mouse skin treated with MSCs and GFs. Although macrophages are the major source of proinflammatory cytokines, neither the CD68 mRNA level nor immunostaining showed a reduction in macrophage infiltration after either MSC or GF treatment. The possibility that treatment with bone marrow-derived MSCs enhances wound healing by increasing the recruitment of macrophages to the wound site has been evoked [37]. Recruited macrophages induce granulation tissue and myofibroblast differentiation during the early stage of the repair and are crucial for the stabilization of vascular structures and the transition of granulation tissue to scar tissue during intermediate stages of repair [28]. MSCs are involved in reprogramming macrophages to an M2 phenotype, through their IL-10 production; they thus enhance wound healing [38]. An important point demonstrated by Horton et al. is that the bone marrow-derived MSC infusion that slows or stops the progression of radiation-induced cutaneous fibrosis is associated with the presence of CD163$^+$ macrophages [39].

Similarly, we have shown that MSC treatment switched the differentiation of macrophages to an M2-like phenotype: we observed specific M2 markers, including the expression of Arg-1, a key feature of M2, and the presence of CD163$^+$ macrophages one week after treatment (day 28 after irradiation). We have shown for the first time that GF treatment also induces an M2 phenotype, just as MSC treatment does. Once recruited to the wound, M2 macrophages promoted angiogenesis, myofibroblast differentiation, and control of follicle size and thus led to the expression of VEGF and TGF-β1 [28,39]. Our data show that MSC and GF treatment increased VEGF expression and that this response occurred earlier in GF-treated skin than in MSC-treated skin.

Although M2 macrophages provide a source for VEGF [28], analysis of the MSC-conditioned medium indicated that MSC secretes many tissue repair mediators, including angiogenic proteins such as VEGFs and epithelial cell stimulatory proteins such as EGF and FGF7 [37]. Physiological levels of these growth factors are critical for ensuring wound healing [40]. Recently, Séguier et al. showed in vitro that the immunomodulatory effects of GFs involve VEGF secretion [21]. We showed here that VEGF, FGF7, and EGF were overexpressed earlier in GF-treated skin than in MSC-treated skin. These molecular events may contribute to the temporal difference in the effects of GF and MSC treatment.

This work is the first to demonstrate that wound healing is significantly accelerated by local injection of GFs, compared with MSC treatment. This effect is temporally associated with ECM remodeling, growth factor production, and macrophage polarization.

Using BM-MSC-derived conditioned medium previous report demonstrated that BM-MSC enhances wound healing through paracrine pathways and the growth factors and cytokines released together to modulate the local environment, affecting the proliferation, migration, differentiation, and functional recovery of resident cells [37]. The mechanism of GF therapeutic effect on wound healing such as MSC therapy involved inflammatory modulation associated to a switch of macrophages to an M2-like phenotype and an ECM remodeling is reinforced by previous observations where GF secretion factors inhibited dendritic cell differentiation [21].

The remodeling efficiency of GF has been described in treatment of arterial aneurisms in rabbit [23]. We have showed in Fig. 1 that MSC and GF expressed some growth factors and mediators implicated in anti-inflammatory response, angiogenesis, and remodeling. As compared to MSC, GF overexpressed fibroblast activation protein a and S100A4 implicated in fibroblast activation and TGF-β2, essential for hair follicle morphogenesis and regeneration. More particularly, the injected GF overexpressed about 26-fold noggin. Recently reported that the overexpressing noggin in microenvironment display continuous propagation

of hair regenerative waves and highly simplified patterns of hair cycle domains. In addition, bursts of noggin expression in the stem cell niche activated stem cells to proliferate for epithelial renewal [41]. In this way we might hypothesize here that GF by their overexpressing growth factors, which interact with microenvironment healing process and their longer persistence in wound tissue, also previously observed [23] compared to that of bone marrow-derived MSCs contributes to and accelerates tissue regeneration.

These findings indicate that GFs are a still more attractive target than the reference MSCs for regenerative medicine, for they are much easier to collect, can grow in culture, and promote cutaneous wound healing in irradiation burn lesions.

Funding Statement

This work was financially supported by grants from INSERM, Paris Descartes University, Ligue contre le Cancer, Association pour la Recherche sur le Cancer, Big (ANR-09-EBIO-005). The funders had no role in study design, data collection and analysis, decision to publish, or preparation of the article.

Author Disclosure Statement

A. Lafont, J.J. Lataillade, and B. Coulomb are cofounders of the startup ScarCell Therapeutics. The other authors have no conflicts of interest to report.

References

1. Williams JP and WH McBride. (2011). After the bomb drops: a new look at radiation-induced multiple organ dysfunction syndrome (MODS). Int J Radiat Biol 87:851–868.
2. Peter RU. (2005). Cutaneous radiation syndrome in multiorgan failure. BJR (Suppl. 27):180–184.
3. Hill RP, HP Rodemann, JH Hendry, SA Roberts and MS Anscher. (2001). Normal tissue radiobiology: from the laboratory to the clinic. Int J Radiat Oncol Biol Phys 49:353–365.
4. Wu Y, J Wang, PG Scott and EE Tredget. (2007). Bone marrow-derived stem cells in wound healing: a review. Wound Repair Regen 15 (Suppl. 1):S18–S26.
5. Lataillade JJ, C Doucet, E Bey, H Carsin, C Huet, I Clairand, JF Bottollier-Depois, A Chapel, I Ernou, et al. (2007). New approach to radiation burn treatment by dosimetry-guided surgery combined with autologous mesenchymal stem cell therapy. Regen Med 2:785–794.
6. Vojtassák J, L Danisovic, M Kubes, D Bakos, L Jarábek, M Ulicná and M Blasko. (2006). Autologous biograft and mesenchymal stem cells in treatment of the diabetic foot. Neuro Endocrinol Lett 27 (Suppl. 2):134–137.
7. François S, M Mouiseddine, N Mathieu, A Semont, P Monti, N Dudoignon A Saché, A Boutarfa, D Thierry, P Gourmelon and A Chapel. (2007). Human mesenchymal stem cells favour healing of the cutaneous radiation syndrome in a xenogenic transplant model. Ann Hematol 86: 1–8.
8. Agay D, H Scherthan, F Forcheron, N Grenier, F Herodin, V Meineke and M Drouet. (2010). Multipotent mesenchymal stem cell grafting to treat cutaneous radiation syndrome: development of a new minipig model. Exp Hematol 38:945–956.
9. Bey E, M Prat, P Duhamel, M Benderitter, M Brachet, F Trompier, P Battaglini, I Ernou, L Boutin, et al. (2010). Emerging therapy for improving wound repair of severe radiation burns using local bone marrow-derived stem cell administrations. Wound Repair Regen 18:50–58.
10. Leclerc T, C Thepenier, P Jault, E Bey, J Peltzer, M Trouillas, P Duhamel, L Bargues, M Prat, M Benderriter and JJ Lataillade. (2011). Cell therapy of burns. Cell Prolif 44 (Suppl. 1):48–54.
11. Horton JA, KE Hudak, EJ Chung, AO White, BT Scroggins, JF Burkeen and DE Citrin. (2013). Mesenchymal stem cells inhibit cutaneous radiation-induced fibrosis by suppressing chronic inflammation. Stem Cells 31:2231–2241.
12. Gurtner GC, S Werner, Y Barrandon and MT Longaker. (2008). Wound repair and regeneration. Nature 453:314–321.
13. McFarlin K, X Gao, YB Liu, D Dulchavsky, D Kwon, AS Arbab, M Bansal, Y Li, M Chopp, SA Dulchavsky and SC Gautam. (2006). Bone marrow-derived mesenchymal stromal cells accelerate wound healing in the rat. Wound Repair Regen 14:471–478.
14. Han SK, TH Yoon, DG Lee, MA Lee and WK Kim. (2005). Potential of human bone marrow stromal cells to accelerate wound healing in vitro. Ann Plast Surg 55:414–419.
15. Hocking AM and NS Gibran. (2010). Mesenchymal stem cells: paracrine signaling and differentiation during cutaneous wound repair. Exp Cell Res 316:2213–2219.
16. Schatteman GC and N Ma. (2006). Old bone marrow cells inhibit skin wound vascularisation. Stem Cells 24:717–721.
17. Chen JS, VW Wong and GC Gurtner. (2012). Therapeutic potential of bone marrow-derived mesenchymal stem cells for cutaneous wound healing. Front Immunol 3:192.
18. Tomar GB, RK Srivastava, N Gupta, AP Barhanpurkar, ST Pote, HM Jhaveri, GC Mishra and MR Wani. (2010). Human gingiva-derived mesenchymal stem cells are superior to bone marrow-derived mesenchymal stem cells for cell therapy in regenerative medicine. Biochem Biophys Res Commun 393:377–383.
19. Fournier BP, FC Ferre, L Couty, JJ Lataillade, M Gourven, A Naveau, B Coulomb, A Lafont and B Gogly. (2010). Multipotent progenitor cells in gingival connective tissue. Tissue Eng Part A 16:2891–2899.
20. Haniffa MA, MP Collin, CD Buckley and F Dazzi. (2009). Mesenchymal stem cells: the fibroblasts' new clothes? Haematologica 94:258–263.
21. Séguier S, E Tartour, C Guérin, L Couty, M Lemitre, L Lallement, M Folliguet, S El Naderi, M Terme, et al. (2009). Inhibition of the differentiation of monocyte-derived dendritic cells by human gingival fibroblasts. PLoS One 8:e70937.
22. Nishi H, K Ohta, M Takechi, S Yoneda, M Hiraoka and N Kamata. (2010). Wound healing effects of gingival fibroblasts cultured in animal-free medium. Oral Dis 16:438–444.
23. Durand E1, B Fournier, L Couty, M Lemitre, P Achouh, P Julia, L Trinquart, JN Fabiani, S Seguier, et al. (2010). Endoluminal gingival fibroblast transfer reduces the size of rabbit carotid aneurisms via elastin repair. Arterioscler Thromb Vasc Biol 32:1892–1901.
24. Sandler NG, MM Mentink-Kane, AW Cheever and TA Wynn. (2003). Global gene expression profiles during acute pathogen-induced pulmonary inflammation reveal

divergent roles for Th1 and Th2 responses in tissue repair. J Immunol 171:3655–3667.
25. Yates CC, R Bodnar and A Wells. (2011). Matrix control of scarring. Cell Mol Life Sci 68:1871–1881.
26. Tamaoki M, K Imanaka-Yoshida, K Yokoyama, T Nishioka, H Inada, M Hiroe, T Sakakura and T Yoshida. (2005). Tenascin-C regulates recruitment of myofibroblasts during tissue repair after myocardial injury. Am J Pathol 167:71–80.
27. Werner S and R Grose. (2003). Regulation of wound healing by growth factors and cytokines. Physiol Rev 83:835–870.
28. Lucas T, A Waisman, R Ranjan, J Roes, T Krieg, W Müller, A Roers and SA Eming. (2010). Differential roles of macrophages in diverse phases of skin repair. J Immunol 184:3964–3977.
29. Zhang H, G Han, H Liu, J Chen, X Ji, F Zhou, Y Zhou and C Xie. (2011). The development of classically and alternatively activated macrophages has different effects on the varied stages of radiation-induced pulmonary injury in mice. J Radiat Res 52:717–726.
30. Iwahira Y, T Nagase, G Nakagami, L Huang, Y Ohta and H Sanada. (2012). Histopathological comparisons of irradiated and non-irradiated breast skin from the same individuals. J Plast Reconstr Aesthet Surg 65:1496–1505.
31. Klinge U, ZY Si, H Zheng, V Schumpelick, RS Bhardwaj and B Klosterhalfen. (2001). Collagen I/III and matrix metalloproteinases (MMP) 1 and 13 in the fascia of patients with incisional hernias. J Invest Surg 14:47–54.
32. Si Z, R Bhardwaj, R Rosch, PR Mertens, B Klosterhalfen and U Klinge. (2002). Impaired balance of type I and type III procollagen mRNA in cultured fibroblasts of patients with incisional hernia. Surgery 131:324–331.
33. Mackie EJ, W Halfter and D Liverani. (1988). Induction of tenascin in healing wounds. Cell Biol 107:2757–2767.
34. Lee CH, B Shah, EK Moioli and JJ Mao. (2010). CTGF directs fibroblast differentiation from human mesenchymal stem/stromal cells and defines connective tissue healing in a rodent injury model. J Clin Invest 120:3340–3349.
35. Tucker RP, J Ferralli, JC Schittny and R Chiquet-Ehrismann. (2013). Tenascin-C and tenascin-W in whisker follicle stem cell niches: possible roles in regulating stem cell proliferation and migration. J Cell Sci 126:5111–5115.
36. Yi T and SU Song. (2012). Immunomodulatory properties of mesenchymal stem cells and their therapeutic applications. Arch Pharm Res 35:213–221.
37. Chen L, EE Tredget, PY Wu and Y Wu. (2008). Paracrine factors of mesenchymal stem cells recruit macrophages and endothelial lineage cells and enhance wound healing. PLoS One 3:e1886.
38. Maggini J, G Mirkin, I Bognanni, J Holmberg, IM Piazzón, I Nepomnaschy, H Costa, C Cañones, S Raiden, M Vermeulen and JR Geffner. (2010). Mouse bone marrow-derived mesenchymal stromal cells turn activated macrophages into a regulatory-like profile. PLoS One 5:e9252.
39. Yano K, LF Brown and M Detmar. (2001). Control of hair growth and follicle size by VEGF-mediated angiogenesis. J Clin Invest 107:409–417.
40. Maxson S, EA Lopez, D Yoo, A Danilkovitch-Miagkova and MA Leroux. (2012). Concise review: role of mesenchymal stem cells in wound repair. Stem Cells Transl Med 1:142–149.
41. Plikus MV1, JA Mayer, D de la Cruz, RE Baker, PK Maini, R Maxson and CM Chuong (2008). Cyclic dermal BMP signalling regulates stem cell activation during hair regeneration. Nature 451:340–344.

Address correspondence to:
Christine Linard, PhD
Institut de Radioprotection et de Sûreté Nucléaire
B.P. n 17
Fontenay-aux-Roses F-92262
France

E-mail: christine.linard@irsn.fr

Received for publication October 10, 2014
Accepted after revision January 5, 2015
Prepublished on Liebert Instant Online January 13, 2015